UC San Diego
UC San Diego Previously Published Works

Title
Correlation analysis of gap junction lattice images

Permalink
https://escholarship.org/uc/item/9w59v4vf

Journal
Biophysical Journal, 58(5)

ISSN
0006-3495

Authors
Sosinsky, GE
Baker, TS
Caspar, DL
et al.

Publication Date
1990-11-01

DOI
10.1016/s0006-3495(90)82462-0

Peer reviewed

Correlation analysis of gap junction lattice images

G. E. Sosinsky,* T. S. Baker,[‡] D. L. D. Caspar,*[§] and D. A. Goodenough[‖]

*Rosenstiel Basic Medical Sciences Research Center, [§]Department of Physics, Brandeis University, Waltham, Massachusetts 02254-9110; [‡]Department of Biological Sciences, Purdue University, West Lafayette, Indiana 47907; [‖]Department of Anatomy and Cellular Biology, Harvard Medical School, Boston, Massachusetts 02115 USA

ABSTRACT   Fourier averages of connexon images computed from low-irradiation electron micrographs of isolated negatively stained gap junction domains exhibited differences in stain distribution and connexon orientation. To analyze these polymorphic structures, correlation averaging methods were applied to images from negatively stained and frozen-hydrated specimens. For the negatively stained specimens, separate averages over two subsets of connexons with differing degrees of stain accumulation in the axial channel were obtained. Two populations of connexons with opposite skew orientations were distinguishable within a single junctional domain of a frozen-hydrated specimen . Correlation maps calculated using the left- and right-skewed references showed that the selected connexons tend to locally cluster. Using correlation methods to analyze packing disorder in a typical connexon lattice, we estimated the root-mean-square variation in the nearest neighbor pair separation to be ~11% of the lattice constant. Displacements of the connexons relative to each other increased with increasing pair separation in the lattice, rather like a liquid, although long–range orientation order was conserved as in a crystal. These results support the hypothesis that the hexagonal ordering of the connexons results from short-range repulsive forces.

INTRODUCTION

Gap junctions are gated channels that extend across coupled-cell membranes and provide a pathway for intercellular communication (Bennett and Goodenough, 1978). The isolated gap junctions consist of a pair of membrane plaques, each of which contains hexameric connexon units arranged in a hexagonal array. The connexons are paired in the two layers with a common axis of symmetry. They are related by noncrystallographic twofold symmetry axes in the plane of the gap which are skewed by ~8° to the right or left of the lattice axes of the hexagonal array.

Low-irradiation electron microscope images of gap junctions prepared with cationic stains, such as uranyl acetate, show extensive stain accumulation in the axial channel of the connexon. Anionic stains such as phosphotungstic acid are mostly excluded (Baker et al., 1985). Fourier averages of the connexon structure computed from these images reveal significant variations in the extent of stain penetration among samples stained under similar conditions (Baker et al., 1983, 1985). Direct inspection of individual connexons in low-irradiation images exhibiting high contrast (Baker et al., 1985) revealed that stain penetrates different channels in widely varying amounts within a single junction domain. In addition, Fourier processing of gap junction images showed

that opposite skew orientation of connexons may occur within different hexagonal lattice domains. Departures from the ideal hexagonal lattice arrangement of the connexon due to packing disorder are common and often quite large. The coincidence of short-range packing disorder with long-range hexagonal order appears to be an inherent feature of gap junction plaques (Caspar et al., 1977).

Fourier methods for processing electron micrographs provide a convenient and objective way to average out noise in images of regularly ordered specimens. In addition, periodic geometrical constraints can be easily enforced on the unit cell structure to produce an average image. Correlation methods provide a different approach by which images can be averaged (Frank, 1982). These methods allow comparisons to be made between the images of individual unit cells or specified regions within the micrograph, and thereby allow averages to be generated only from regions with demonstrated self-consistency. Correlation methods have proved useful in a number of different applications to ordered two-dimensional arrays: (a) selective image averaging of undamaged, well-preserved units in a lattice (Saxton and Baumeister, 1982; Crepeau and Fram, 1981; Manella and Frank, 1984; Manella et al., 1986); (b) correcting lattice distortions to improve Fourier averaging (Henderson et al., 1986); (c) identifying molecular rearrangements during phase transitions (Dorset et al., 1989); and (d)

Address correspondence to Dr. Sosinsky, Rosenstiel Basic Medical Sciences Research Center, Brandeis University, Waltham, MA 02254-9110.

assessing differences in thicknesses within thin crystalline specimens (Frank et al., 1988). Thus, correlation techniques are ideally suited for examining structural variations within gap junction lattices. In this study, we identify variations in the structure and orientation of the connexon units and measure the extent of disorder in junction lattices.

MATERIALS AND METHODS

Electron microscopy

The micrographs of negatively stained gap junctions analyzed here were recorded during previous studies of specimens that were stained with methylamine tungstate (Fig. 7 B in Baker et al., 1985) or uranyl acetate (Fig. 3 B in Sosinsky et al., 1988).

Micrographs of frozen-hydrated gap junctions were recorded on a JEOL 100B electron microscope equipped with a high-resolution cold stage operating at $\sim -120°C$. Rat liver junction specimens were adsorbed onto carbon grids and quickly frozen in liquid nitrogen. Micrographs were recorded under low-irradiation conditions ($\sim 5e^-/Å^2$ at a nominal magnification of 40,000).

Image processing

Micrographs were digitized at 25-μm steps on a scanning densitometer (model P1000 Photoscan; Optronics International Inc., Chelmsford, MA) and displayed on a raster graphics terminal. Thus, the pixel spacings in the digitized images were nominally 6.25 Å for the 40,000 magnification micrographs. Regions of junction images selected for further analysis were extracted from the displayed digital image by interactive graphics procedures. All computations, including Fourier transformations were carried out on a VAX 11/780 minicomputer (Digital Equipment Corp., Marlboro, MA). Fourier averaging of crystalline hexagonal arrays was performed according to established procedures (Baker et al., 1983, 1985).

The averaging procedures we used (Fig. 1) were adapted from the methods developed by others (Saxton and Baumeister, 1982; Manella et al., 1986; Frank et al., 1988). Generally, the best references were obtained not from an original (unfiltered) image, but from an image that was processed by Fourier methods (Baker, 1981) to remove high- and low-frequency noise and to locally average images of adjacent unit cells (Fig. 1, step 3A). High spatial frequencies in the images, which are due predominantly to random noise, were suppressed by multiplying the Fourier transforms with a function that is circularly symmetric about the transform origin and has a value of unity out to $\sim 1/17$ Å and falls smoothly to zero at a spacing of $\sim 1/15$ Å. Low-frequency noise, arising from nonuniform staining or uneven sample or ice thickness, was removed by a similar Fourier masking procedure that eliminated transform data below spacings of 1/200 Å. For some micrographs, the connexon images in the hexagonal lattice were locally averaged by multiplying the Fourier transform of the lattice by a periodic mask of aligned, Gaussian weighted holes. The extent of local averaging in the image was confined to a region ~ 2-3 unit-cell repeats wide by adjusting the holes in the Fourier filter mask to a diameter $\sim 1/3$-1/2 of the reciprocal lattice repeat distance.

Correlation averaging

Reference images, corresponding to an area containing a single connexon or a connexon and its six nearest neighbors, were extracted from
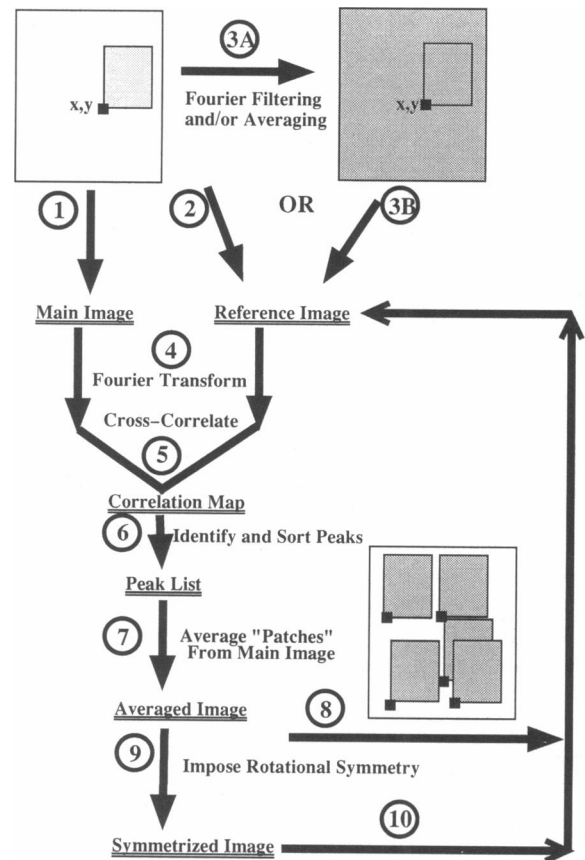

FIGURE 1 Schematic diagram of correlation averaging procedures. The outlined methods are similar to those described by Saxton and Baumeister (1982). Details are given in Materials and Methods.

the original unprocessed image (Fig. 1, step 2) or from a filtered image (Fig. 1, step 3B) to initiate the correlation averaging procedure. The Fourier transforms of the reference and main image (Fig. 1, step 4) were multiplied together and back transformed (Crepeau and Fram, 1981) to compute a cross-correlation map (Fig. 1, step 5). Values in the correlation map were sorted by magnitude in descending order (Fig. 1, step 6). This list of peak values was searched to identify maxima in the correlation map separated by a minimum distance comparable to the unit cell dimensions. The separation threshold applied in this study was 60 Å. This distance was small enough to assure that connexon pairs that were somewhat closer than the average ~ 80-85-Å lattice constant would not be eliminated.

The positions of the peaks identify the locations of regions in the main image that correlate well within the reference image. The magnitude of each peak at a position r is a measure of the correlation between the identified region and the reference. The correlation coefficient for a displacement r between the reference origin and that of the main image ($CC(r)$) is defined as

$$CC(\mathbf{r}) = \frac{\sum_i (\rho_1(x_i) \cdot \rho_2(\mathbf{r} + x_i))}{\sqrt{(\Sigma \rho_1^2) \cdot (\Sigma \rho_2^2)}},$$

where ρ is the density value at an image point x_i minus the average density of all the pixels. The summation is taken over the product of the

density at each point in the area of the reference image ($\rho_1[x_i]$) and that of each corresponding point in the same area of the main image ($\rho_2[r + x_i]$) measured for the displacement vector r. The value of the CC is unity if the two images are identical and zero if they are unrelated. The power of the image summed over the areas compared equals $\Sigma\rho^2$, and this should be independent of origin for an integral number of unit cells in a periodic structure.

Averages were computed from the sum of the 50–100 areas the size of the reference that correlated best with the reference (Fig. 1, *step 7*). Because the gap junction domains that were examined typically contain at least 400 unit cells, 75% or more of the connexon images were excluded from the correlation averages. The correlation average was used as a new reference image for a subsequent cycle of correlation averaging (Fig. 1, *step 8*) or, alternatively, it was rotationally averaged to enforce perfect sixfold symmetry about the connexon axis (Fig. 1, *step 9*) and then used as a new reference (Fig. 1, *step 10*).

Analysis of disorder in junction lattice domains

Lattice disorder within a gap junction domain was analyzed from the positions of the connexon centers in the original image. These positions were obtained by taking a single connexon image as a reference and cross-correlating it with the original image. Peaks, corresponding to the number of connexons in the image, were selected from the correlation map according to the magnitude and minimum separation criteria. These peaks were normalized to a constant value and the remaining values were set equal to zero. The squared Fourier transform of this map of the connexon positions was computed (Fig. 8 *A*) and the intensities were circularly averaged about the transform origin to produce a one-dimensional intensity distribution corresponding to a circularly averaged diffraction pattern (Fig. 8 *D*). The diffuse background of this averaged diffraction pattern increases smoothly as a function of the reciprocal space coordinate R to a plateau I_{max} for large R. The diffuse intensity $I_{diff}(R)$ was fitted to the complement of a Debye function: $I_{diff}(R) = I_{max}(1 - e^{-(2\pi\delta R)^2})$, where δ^2 is the mean square random displacement of a connexon center from the origin of the locally fitted average hexagonal lattice. The rms variation in the nearest neighbor pair separation is $\sigma = \sqrt{2}\delta$.

Correlations in the displacements of neighboring connexons were assessed by calculating the Patterson (autocorrelation) function (Fig. 8 *C*) from the map of connexon positions (Fig. 8 *B*). The standard deviation of the breadth of the autocorrelation maxima, sampled along the horizontal axis (Fig. 8 *E*) was estimated by a program that fitted each peak to a Gaussian. The ratio of the standard deviation of each Gaussian peak, σ, to the lattice constant, a_o, was plotted as a function of distance from the origin of the autocorrelation map (Fig. 8 *F*).

RESULTS

Variations in the structure of the repeating unit

The ability of correlation techniques to distinguish structural variations is conveniently illustrated with model simulations (Fig. 2). We generated a model crystal structure with 240 unit cells by placing motifs, selected at random from one of three similar but distinct motifs, at each of the points of an ideal rectangular lattice. The different motifs were pictures of right hands, with the

index finger pointing to the right in three different positions (downward, upward and directly to the right as identified by the reference images 1–3 in Fig. 2 *A*). These three motifs were used as correlation references to compute separate averages, each derived from the 25 unit cells from the crystal model that correlated best with the respective references. The correlation averages (Fig. 2 *C*1–2 *C*3) are compared to a Fourier average of all 240 unit cells (Fig. 2 *C*4). As expected, the correlation method faithfully discriminates and sorts the different motifs into separate, distinct averages, whereas the Fourier procedure produces an "average" motif in which the common features (wrist and fist) are recovered but the variable feature (index finger) smears out. The CC is 0.86 for the motif 1 versus 2, and 0.89 for motif 1 versus 3 in Fig. 2 *A*. These values indicate that the finger contributes ~11–14% of the total power within each motif image.

The effects of noise on the ability of correlation methods to distinguish differences in similar motif images were also examined by model simulations (Fig. 2 *B*). Gaussian noise, with about five times the power of the "signal," was added to the model image (Fig. 2 *A*) to represent a noisy image of a crystalline specimen (Fig. 2 *B*). References that correspond to the same motifs selected from Fig. 2 *A* were used to compute three correlation averages (Fig. 2 *D*1–2 *D*3). A Fourier average was also computed (Fig. 2 *D*4). The CC for motif 1 versus 2 in Fig. 2 *B* was 0.19 and for 1 versus 3, the CC was 0.08. The CCs for the noise components of these two pairs running against each other were 0.05 and -0.07, respectively. The mean value of the noise cross-correlation coefficient, averaged over many pairs of unit cells, is necessarily zero for random noise; however, the root-mean-square value of the CC for a sample area is finite, being determined by the number of pixels in the reference area and the mean square noise level. The substantial difference in the CC for motif 1 versus 2 compared to 1 versus 3 is within the range expected for the fluctuations in the noise. For noise with five times the power of the image motif, the mean CC comparing identical motifs with different noise components should be 0.167; and for the different motifs with 86–89% of the image in common on the noisy background, the mean CC should be ~0.14. The mean cross-correlation noise level of ~ ±0.06 can increase or decrease the individual values of the CC for the noisy motifs.

In spite of the high noise level in the starting model (Fig. 2 *B*), significant improvement in the signal-to-noise ratio was observed in the correlation averages (Fig. 2 *D*). Different motifs could be distinguished, even though the mean fluctuations due to noise are about twice the discriminating difference in the mean CCs because, on the average, the identical motifs have the larger CC. In the Fourier average (Fig. 2 *D*4) the background noise was
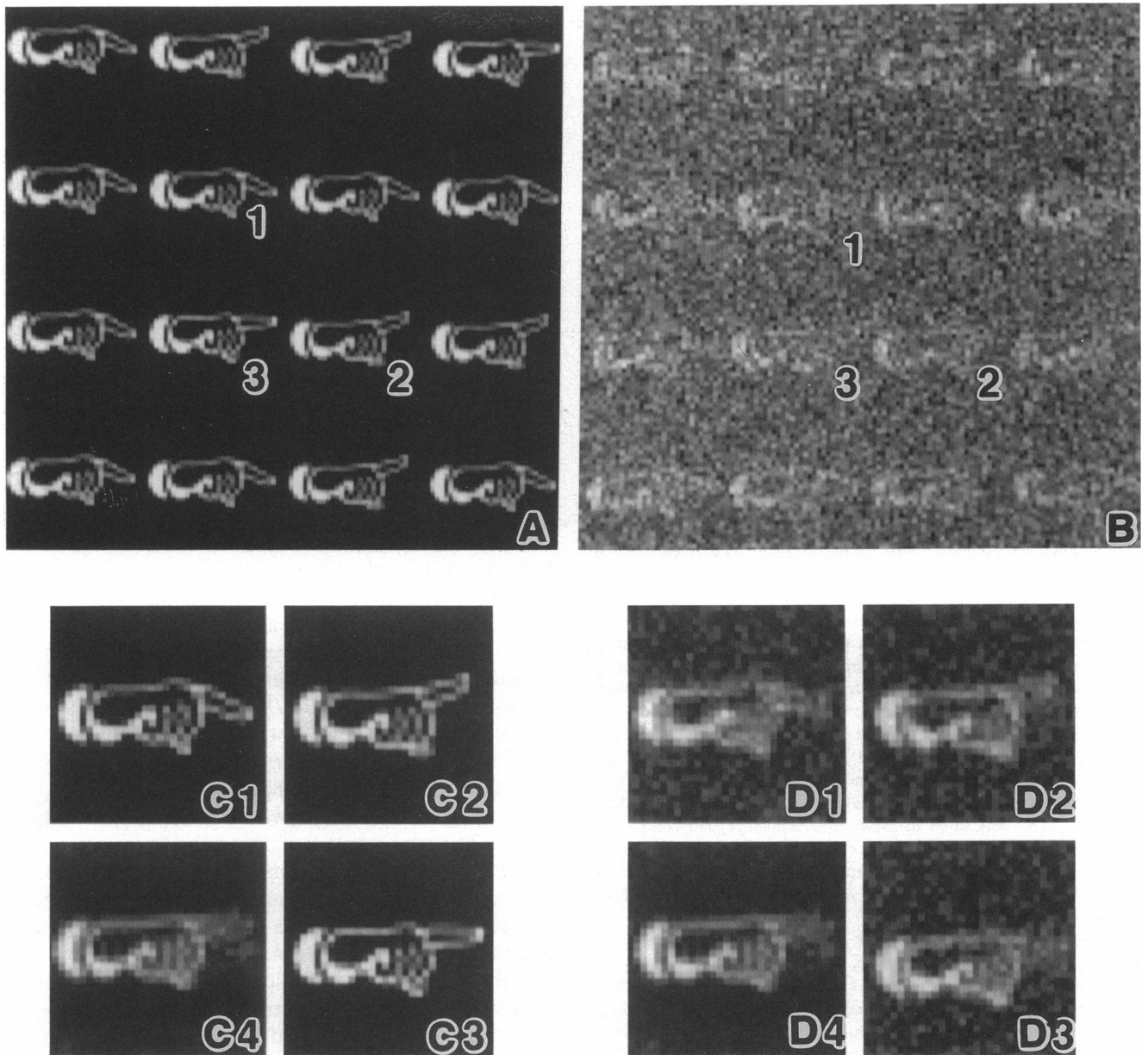
FIGURE 2   Detection of structural variations by use of correlation methods. (*A*) Part of a model crystal structure constructed with 240 righthand motifs positioned on an ideal, rectangular lattice. The motif at each lattice point was randomly chosen from a set of three similar motifs that differ only in the orientation of the index finger. (*B*) Same as (*A*) with noise added to simulate real data. (*C1–C3*) Averages, each computed from the 25 motif images that best correlate with the three different reference images, labeled 1, 2, and 3 in (*A*). (*C4*) Fourier average of the entire model image (240 unit cells), illustrating the smearing of the index finger feature. (*D1–D4*) Same as (*C1–C4*) but from the noisy image (*B*). Although the index finger is smeared in the Fourier averages (*C4* and *D4*), the different orientations of the index finger are revealed in the correlation averages (*D1–D3*) from the 25 motif images that respectively correlate most strongly with those references.

reduced to a greater extent than that in the correlation averages because there were approximately nine times more unit cells contributing to the Fourier average. Consequently, the wrist and fist features were more enhanced in the Fourier average compared to the correla-

tion averages, although the Fourier average of the index finger was smeared as before (cf. Fig. 2 *C4*).

Similar Fourier and correlation averaging procedures were applied to minimal-irradiation images of negatively stained and frozen-hydrated gap junction specimens. In

Fourier averages, the connexons in a junction domain appear to pack in either a right- or left-handed skew orientation (defined by the position of the local twofold axes of the connexon which are parallel to the membrane plane and rotated ~8° to the right or left of the hexagonal lattice axes; see Baker et al., 1983). However, examination of images of negatively stained and frozen-hydrated junctions with correlation procedures unexpectedly revealed that connexons in single–hexagonal lattice domains pack with a mixture of the two orientations, although one generally predominates.

Analysis of an image of an unstained junction domain illustrates the mixture of skew orientations (Fig. 3). Reference images were obtained from small regions of a micrograph that was Fourier-filtered to impose local averaging and reduce noise. References with connexons skewed either left or right could not be located by eye in unfiltered images but could be identified in the locally
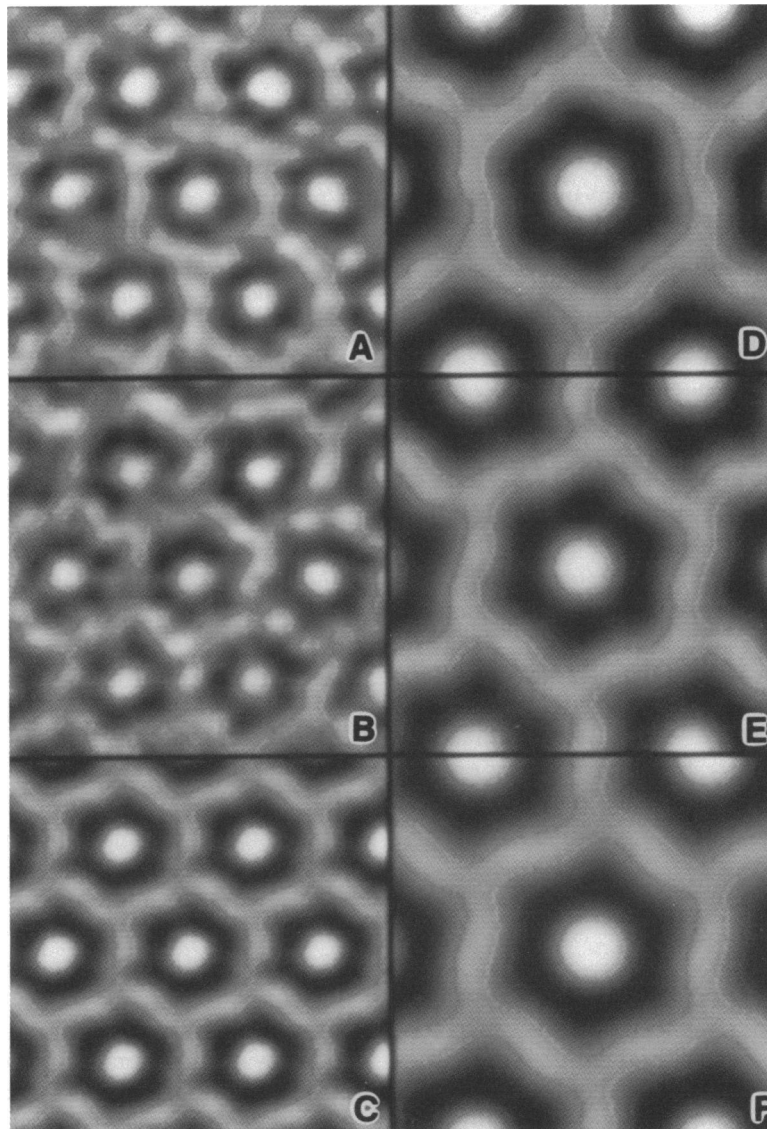

FIGURE 3 Detection of connexon skew orientations in a frozen-hydrated junction domain. (A and B) Correlation averages obtained by use of reference images selected from separate areas of a filtered image of one domain. The two averages, each obtained from the sum of 50 subareas, differ in the orientation of the connexons in the hexagonal array. Connexons are skewed left in A and right in B. (C) Fourier average of the entire domain (~900 unit cells). (D–F) Sixfold, rotationally symmetrized averages of (A), (B), and (C), respectively. The right-hand skew of the connexon in the Fourier average (F) indicates that this orientation predominates in the domain that was analyzed. Similar results were obtained for negatively stained junctions (data not shown).

averaged image. Representative examples of correlation averages obtained from each of the two types of reference image, along with the global Fourier average, are compared in Fig. 3, A–C. These averages were symmetrized to enforce perfect sixfold symmetry at the connexon center (Fig. 3 D–F). The CC of Fig. 3 D versus 3 E is 0.90. Thus, the hexagonally symmetric features that distinguish the left- (Fig. 3 D) from the right- (Fig. 3 E) skewed orientation constitute 10% of the power of the average connexon image. Because the Fourier average (Fig. 3 F) has the connexon skewed to the right, the junction domain used in this example must have contained connexons packed predominantly with a righthand skew orientation.

A second type of variation detected in connexon images arises from differences in the amount of stain that accumulates in the axial channel of the connexon. Cationic uranyl stains tend to penetrate the channels more extensively than negatively charged tungstate or molybdate ionic complexes (Baker et al., 1985). However, there is considerable variation in the contrast at the center of individual connexons within a junction domain stained under uniform conditions. Analysis of a junction domain stained with uranyl acetate illustrates this observation (Fig. 4). Separate correlation reference images, each containing a single connexon surrounded by six neighbors, were selected to distinguish extremes of stain penetration in the channel. As expected, the correlation averages (Fig. 4 A–B) show significant differences in contrast at the connexon center. The Fourier average (Fig. 4 C) has an appearance intermediate to that of the two correlation averages, indicating that there is considerable variation in the channel staining within a single junction domain. The CC of the sixfold symmetrized correlation averages of the connexons with dark and light centers (Fig. 4 D versus 4 E) is 0.83. Thus, the very localized differences in axial staining produce substantial changes in the image that can be systematically distinguished by correlation averaging.

Distribution of variable connexons within junction lattices

Correlation maps identify regions in the original image most similar to the reference. Thus, with different reference images, the distribution of different motifs (e.g., different skew orientation or different channel staining) within an individual gap junction domain can be examined. A correlation map, derived from each of the two reference images from the uranyl acetate-stained junction, reveals the distribution of connexons with high (Fig. 5 A) or low (Fig. 5 B) channel contrast. The positions of the strongest 50 peaks in each map, corresponding to the regions summed to produce the correlation averages (Fig. 4 A and B), were highlighted with white dots (Fig. 5 A

and B). The image of the unstained junction was similarly analyzed to distinguish connexons skewed to the left (Fig. 5 D) or to the right (Fig. 5 E) in the hexagonal array.

The positions of the 50 highest peaks in each pair of correlation maps were overlayed (Fig. 5, C and F) to examine how the different types of connexon segregated. Most of the peaks were found to lie at unique lattice positions and there was some tendency for connexons of a given type to cluster together. However, the different connexons were not confined to specific regions within the domain. A few connexons were identified at positions common to both correlation maps, where the peaks superimpose (i.e., where crosses and boxes overlap, Fig. 5, C and F). Presumably, such connexons are characterized by features common to both reference images, and these features must be strong compared to those that distinguish the references. Thus, correlation procedures failed to provide unequivocal classification of these connexon images. Similar ambiguity was observed in the classification of some of the noisy hand motifs in Fig. 2, which was due to noise variations in the magnitudes of the CC maxima.

Correlation averaging of individual connexon images

Reference images of single connexons were used to compute correlation averages. Individual connexons are clearly visible in a high contrast micrograph (Fig. 7 A) of a junction membrane stained with methylamine tungstate and recorded by low-irradiation procedures (Baker et al., 1985). Three different references (Fig. 6, A, D, and G) were chosen to compute correlation averages of the connexon (Fig. 6, B, E, and H), each of which included only 10 connexon images from the original micrograph. One reference (Fig. 6 A) was obtained from a sixfold rotationally symmetrized correlation average, computed by starting with a single connexon reference and summing the 400 best areas. The other two references (Fig. 6, D and G) were selected directly from the original image from connexons showing extremes of stain penetration in the channel. Although the noise in the averages was still high, the sixfold rotational symmetry of each connexon was evident (Fig. 6, B, E, and H). Enforcing sixfold symmetry on the averages helped clarify the differences between them (Fig. 6, C, F, and I). Features such as the stain that outlines the six-lobed connexon appear similar in all averages, whereas the amount of stain in the channel differs.

Attempts to average single-connexon images by correlation procedures with images of uranyl acetate-stained junctions proved unsuccessful. Apparently, false correlations occur as a result of the concentration of stain in the channel and around the periphery of the connexon.
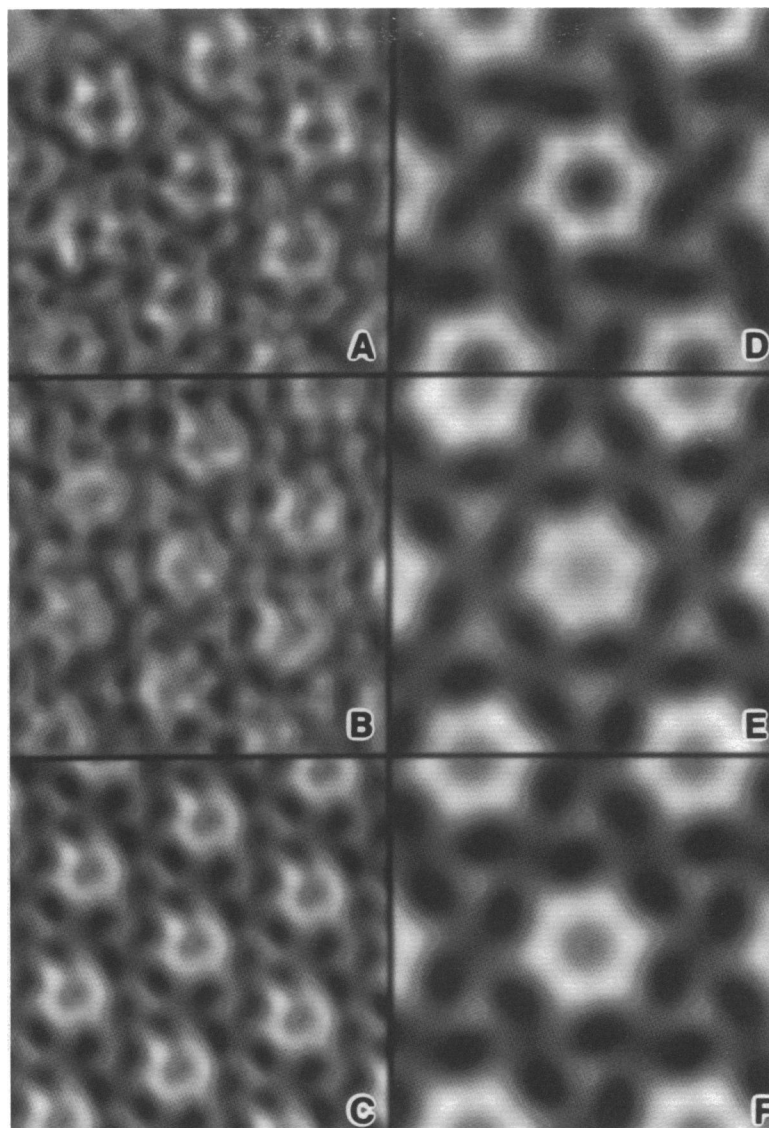
FIGURE 4 Detection of differences in contrast at the center of connexons within a junction domain stained with uranyl acetate. (*A* and *B*) Correlation averages obtained by use of reference images selected from separate areas of a filtered image of one domain. The two averages, each obtained from the sum of 50 separate "patches," differ primarily in the contrast at the center of the connexon. (*C*) Fourier average of the entire domain (~1,200 unit cells) from which the correlation averages (*A*) and (*B*) were obtained. (*D–F*) Sixfold, rotationally symmetrized averages of (*A*), (*B*), and (*C*), respectively. Connexons in the Fourier average (*F*) appear to have an intermediate level of stain accumulation at the connexon center compared to the extremes represented by (*D*) and (*E*).

With methylamine tungstate, most of the stain surrounds the periphery of the connexon and very little penetrates the channel.

Analysis of lattice disorder in a gap junction domain

Disorder in the gap junction lattice was analyzed in the specimen stained with methylamine tungstate because the positions of the connexon centers could be reliably identi-

fied in this micrograph (Fig. 7 *A*) by correlation methods. The boundary between separate junction domains was visible in the original micrograph and was even more clearly revealed in a cross-correlation peak map of a selected area superimposed on the micrograph (Fig. 7 *B*) and in the peak map alone (Fig. 7 *C*). The two hexagonal lattice domains of the part of the gap junction shown in Fig. 7 are rotated by ~30° relative to each other.

Lattice disorder was quantitatively assessed in a domain from the region illustrated in Fig. 7 *B*. A portion of
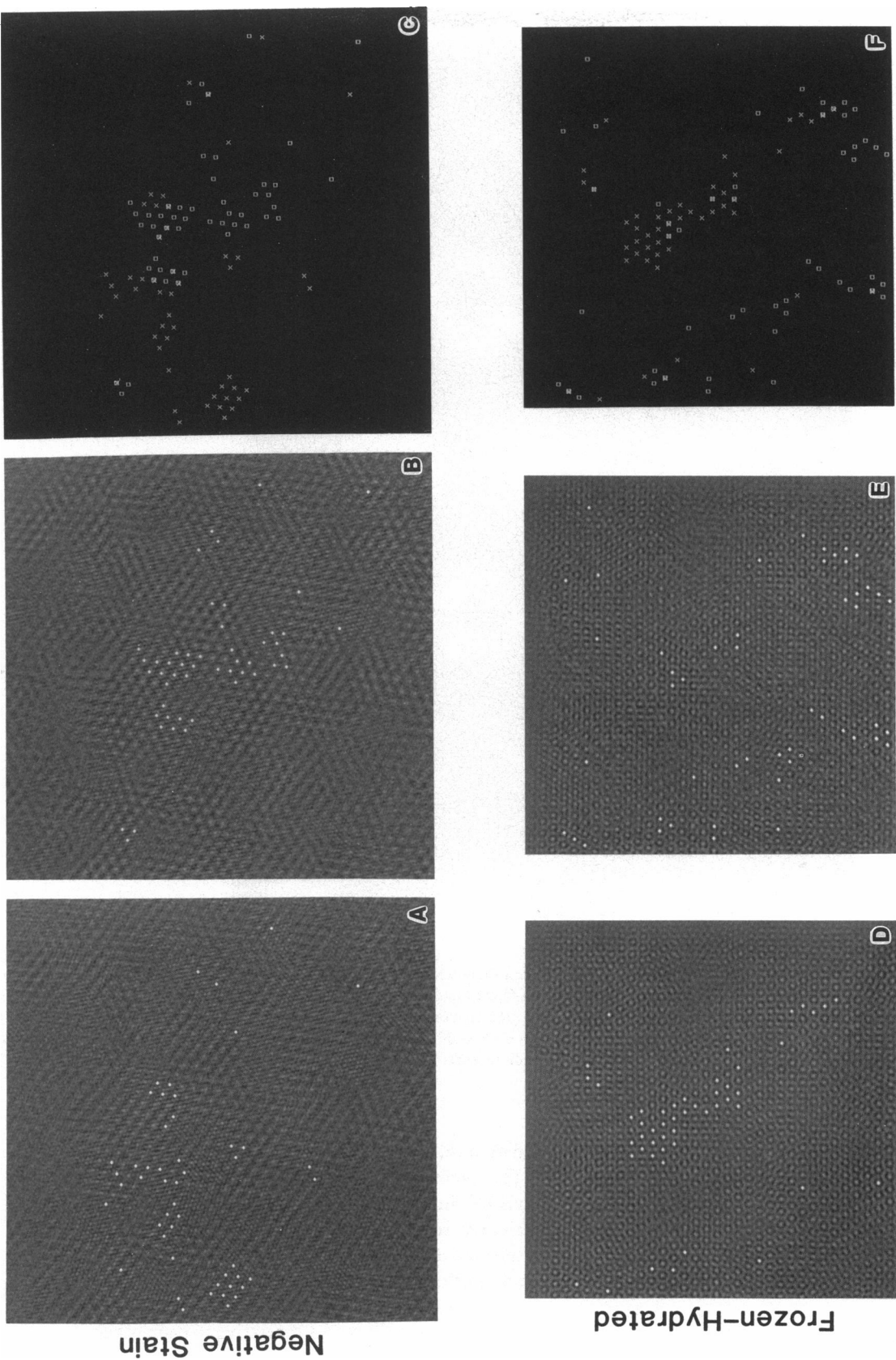
FIGURE 5 Correlation maps. (*A* and *B*) Correlation maps computed from the image of the stained junction, with reference images of connexons with darkly stained (*A*) or lightly stained (*B*) channels. (*D* and *E*) Correlation maps computed from the image of the unstained, frozen-hydrated junction, with reference images containing connexons oriented with a left skew (*D*) or a right skew (*E*). The junction domains analyzed by correlation averaging procedures contained 400 or more unit cells. White dots mark the positions of the 50 strongest peaks in each correlation map and identify the regions in each domain selected to form the correlation averages displayed in Figs. 4 *A*, 4 *B*, 3 *A* and 3 *B*, respectively. (*C*) Superposition of the 50 peaks in (*A*, crosses) and the 50 peaks in (*B*, open squares), demonstrating the distribution and overlaps of areas used to calculate two correlation averages. (*F*) Superposition of the 50 peaks from the maps shown in (*D*, crosses) and (*E*, open squares).
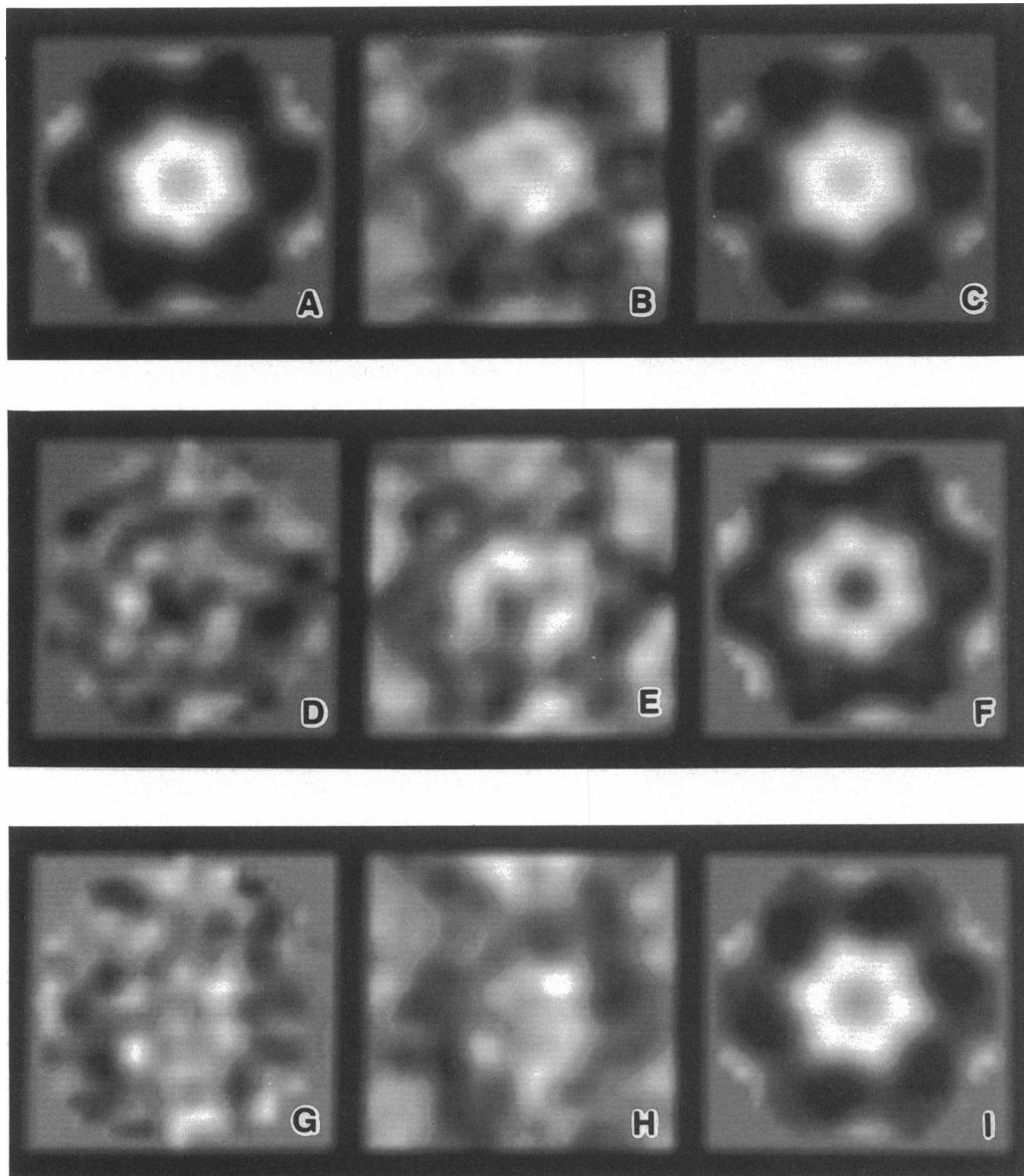
FIGURE 6   Correlation averaging of single connexons. Reference images (*A*, *D*, and *G*), consisting of a single connexon and a small portion of each of the six neighboring connexons, were used to compute correlation averages (*B*, *E*, and *H*) from an image of a junction domain stained with methylamine tungstate (shown in Fig. 7 *A*). (*A*) A sixfold, rotationally symmetrized correlation average of 400 unit cells from the junction image (*A*) was used to compute a correlation average (*B*) from just ten connexon images. Similar correlation averages (*E* and *H*) were produced from reference images of connexons with either high (*D*) or low (*G*) contrast in the center. (*C*, *F*, and *I*) Sixfold, rotationally averaged images of *B*, *E*, and *H*, respectively.

the cross-correlation map (Fig. 7 *C*) consisting of ~1,400 peaks corresponding to connexons packed in a uniformly oriented hexagonal array was redisplayed in Fig. 8 *B* (which has been rotated 90° clockwise relative to Fig. 7 *C*). The Fourier transform of this map of peak positions was computed and displayed on two different intensity scales (Fig. 8 *A*), one emphasizing the intense, normal Bragg diffraction from the approximately periodic array

(*left half*) and the other emphasizing the diffuse variational diffraction due to irregularities in the packing (*right half*). Fig. 8 *D* shows how the diffuse, background scatter in the circularly averaged intensity profile was closely fitted with a Gaussian curve whose standard deviation is proportional to the root-mean-square (rms) variation in the hexagonal lattice packing. The measured rms displacement from the locally fitted hexagonal lattice
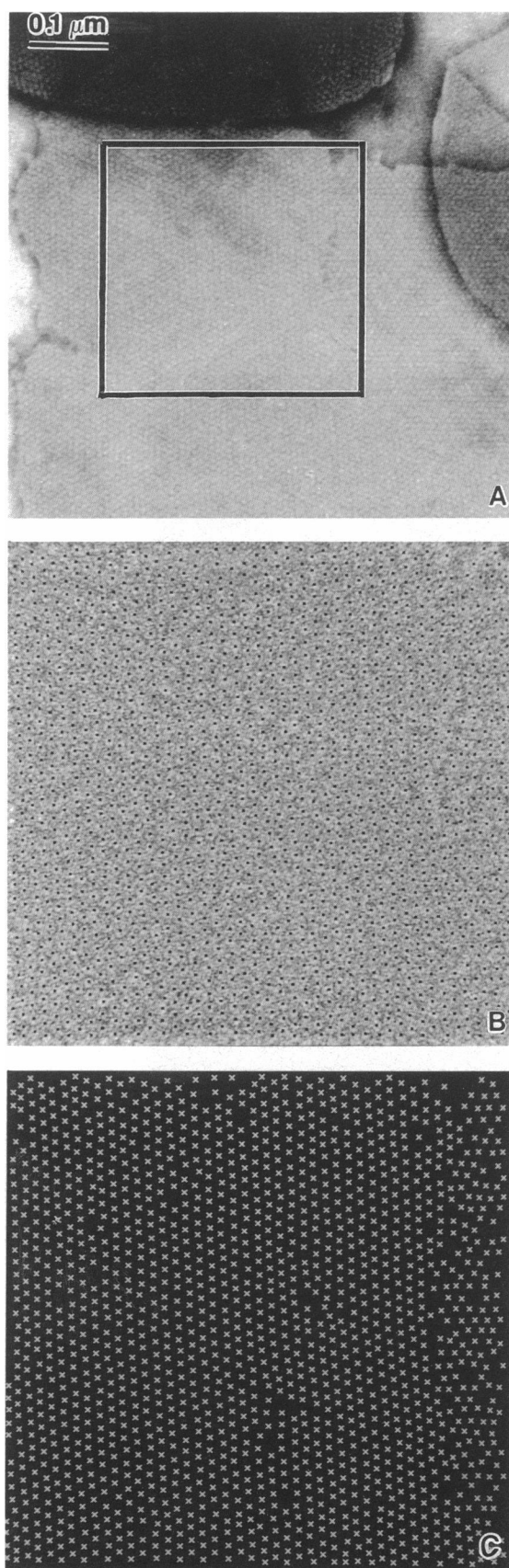
with $a_0 = 80$ Å was $\delta = 6.05$ Å, corresponding to an rms variation in nearest neighbor pair separation of $\sigma = 8.56$ Å, which is 10.7% of the mean lattice constant.

We also assessed the short-range order in the junction domain by computing the autocorrelation function of the map of peak positions (Fig. 8 C). A one-dimensional plot of the data along the horizontal axis of the autocorrelation function shows that the width of successive peaks increases with increasing distance from the origin (Fig. 8 E). (The linear decrease in peak area with increasing separation is a mathematical characteristic of the autocorrelation function of finite size arrays.) A plot of the standard deviation of the peak widths as a function of distance from the origin of the autocorrelation function (Fig. 8 F) was fit by a least-squares procedure to obtain the relation $\sigma_n = (7.94 + 0.57n)$ Å for the standard deviation of the nth nearest neighbor pair correlation peak. The rms variation in the nearest neighbor pair separation, as measured by σ_1, the mean width of the first peak in the autocorrelation function, was 8.51 Å. This value is in good agreement with the value 8.56 Å calculated from the circularly averaged transform of the connexon positions as shown in Fig. 8 D. The small difference between the values might indicate that there is slightly better order among neighboring connexons in the horizontal direction than in the other lattice directions.

Fig. 8 F shows that the widths of the autocorrelation peaks increase linearly with separation over the measured range. Thus, the connexon array is not, strictly speaking, a crystal because the autocorrelation function of a "crystal" by definition does not diverge. At large separations the connexon packing resembles a liquid in the sense that the autocorrelation function peaks merge to give a uniform probability for separations greater than some characteristic coherence distance. From the slope of the peak widths as a function of separation plotted in Fig. 8 F, the coherence distance is ~40 times the lattice constant.

DISCUSSION

We have used correlation methods to analyze variations in the structure, orientation, and packing of the connex-

FIGURE 7 Identification of crystalline disorder and defects in junction images. (A) Low magnification view of a gap junction membrane stained with methylamine tungstate. (B) Enlargement of the region boxed in (A) that shows an extended hexagonal domain on the left and a part of a differently oriented hexagonal domain on the right. Black dots mark the positions of the connexons as determined by correlation analysis with a single connexon image used as a reference. (C) Same as (B) minus the junction image and with the correlation peak positions identified by white crosses. The hexagonal lattices of the two domains are rotated by 30° (or equivalently 90°) relative to each other. Various crystal lattice defects (e.g., missing connexons, deviations of connexons from ideal lattice positions, and incomplete rows of connexons) are evident. The magnifications of (B) and (C) are twice that of (A).
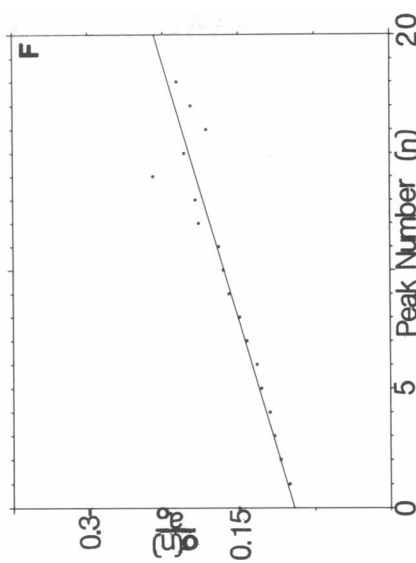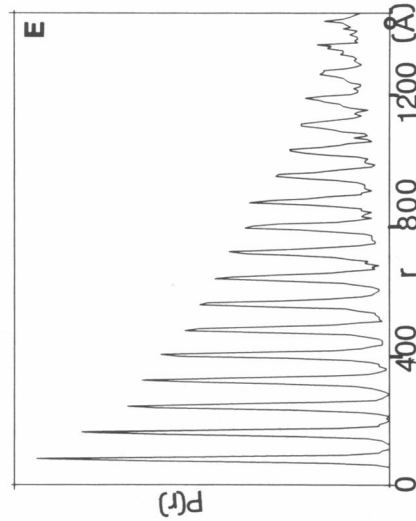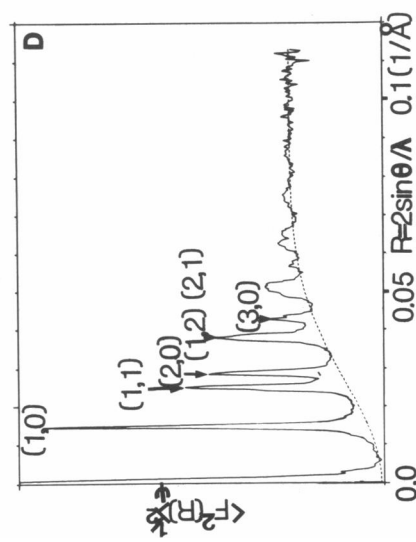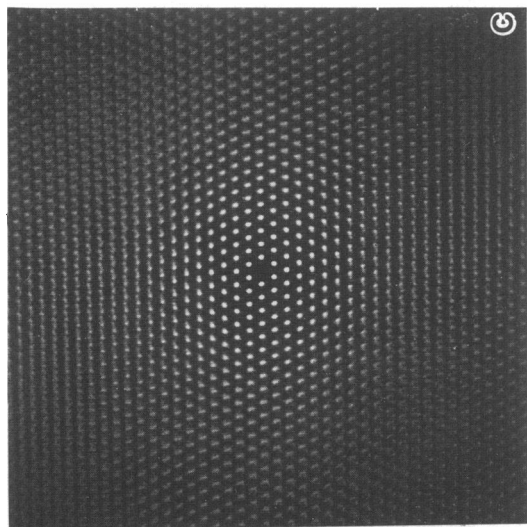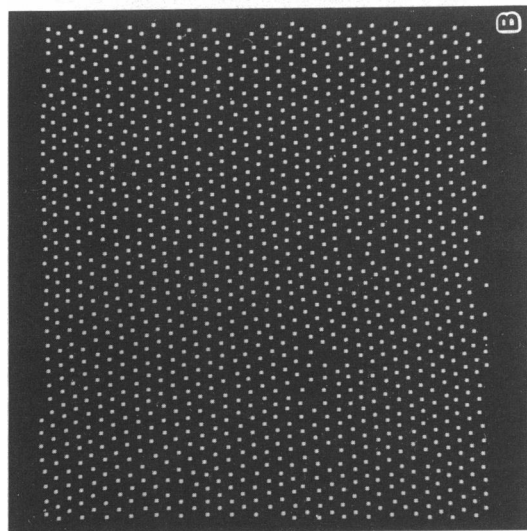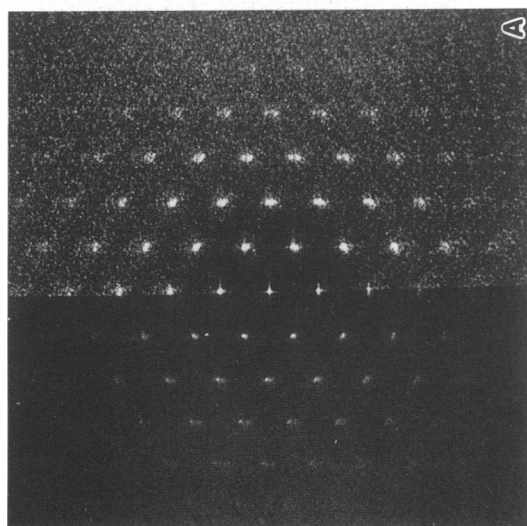
FIGURE 8 Analysis of disorder in connexon packing. (*A*) Diffraction pattern computed from *B*, scaled to show the strong, coherent scatter (*left half*) arising from periodic features in *B*, and scaled to show the diffuse scatter (right half) caused by deviations from the ideal lattice. (*B*) Correlation peak map of a portion of the large domain shown in Fig. 7 *B* (orientation is rotated 90° relative to 7 *C*). (C) Autocorrelation function of *B*, with the origin peak removed. (*D*) One-dimensional profile of the intensity distribution (*A*), circularly averaged about the origin. Indices for all Bragg reflections out to the third order are given. The dotted curve represents the complement of a Debye function $I_{diff}(R) = I_{max}(1 - e^{-(2\pi dR)^2})$ fitted to the diffuse background. (*E*) Plot of the horizontal axis of the autocorrelation function (*C*). Peaks, corresponding to connexon pairs separated by lattice repeats, gradually broaden at increasing pair separation distances. (*F*) Standard deviations of the autocorrelation peaks divided by the lattice constant ($a_o = 80$ Å) in *C* plotted as a function of distance from the origin of the autocorrelation function. The standard deviation of the nth nearest neighbor correlation peak, σ_n, was obtained by fitting a two-dimensional Gaussian to each peak along the horizontal axis. The line fit to the data is given by the equation $\sigma_n = (7.94 + 0.57n)$ Å.

ons in gap junction membranes, and have also assessed the limitations on discrimination of these variations imposed by noise in the micrographs. For noise-free images of arrays of related motifs, there is no problem in discriminating identical objects from those that are slightly different by calculation of the cross-correlation function. Intrusion of noise introduces differences in the images of identical objects which reduce the mean value of the CC peak and lead to a spread of these peak values. Thus, discrimination among similar noisy images by cross-correlation methods may no longer be unique.

Random noise variations of mean square amplitude $\overline{v^2}$ per pixel superimposed on identical images, each consisting of N pixels of mean square amplitude $\overline{p^2}$, will lead to a standard deviation for the CC maxima equal to $(\overline{v^2}/\overline{p^2}N)^{1/2}$ times the mean peak value of the CCs, evaluated relative to a noise-free reference. For noise with four times the image power ($\overline{v^2} = 4\overline{p^2}$) and a reference image area of $N = 100$ pixels, the standard deviation in the peak values would be 20% of the mean CC. (The mean CC would be reduced by the factor $(1 + \overline{v^2}/\overline{p^2})^{-1/2}$ compared to the noise-free value.)

As shown by the example of the array of noisy hand motifs (Fig. 2), it is possible to discriminate similar images whose mean CC maxima for identical and different pairs differ by less than half the standard deviation of the mean. A histogram of the CC peak values for an array of two similar noisy motifs correlated with one of the motifs as reference would consist of two overlapping Gaussians. Those images, whose CC peak values are greater than the mean, will be made up of more identical than different motifs. Thus, the average of these images will resemble the reference more closely than the global average. Superposition of the cross-correlation maps of the peak positions calculated for references corresponding to the two motifs would necessarily show some overlaps. The fraction of overlaps will depend on the difference in the mean CCs for identical and different pairs, on their standard deviations and on the cut-off in the CCs taken to construct the maps.

The plot of the positions of the CC maxima, for a noise-free array of identically oriented identical motifs correlated with the repeating unit reference, determines exactly the coordinates of all the motifs. For noisy images, the highest peaks in the CC map no longer necessarily correspond exactly to the motif coordinates. The variation in highest peak positions from the actual motif coordinates depends on noise fluctuations in the CC values and on the shape of the CC maxima.

Variations in connexon images

Connexon positions in micrographs of gap junction membranes cannot, in general, be determined by cross-

correlation with a single connexon reference image because of the relatively high noise level. In low-irradiation micrographs of unstained, frozen-hydrated gap junctions, the noise level is much higher than the mean image contrast, which makes it difficult to distinguish individual connexons. In low-irradiation micrographs of uranyl acetate-stained junctions, the image contrast is relatively high; but, because the stain concentrations at the center and periphery of the connexon are similar in size and density, the CC with a single connexon reference has subsidiary maxima (displaced by the separation of the central and peripheral features) which may differ in magnitude from the origin peak by less than the noise level. Mean coordinates of the connexons in well-ordered lattice domains can be determined from micrographs of frozen-hydrated and uranyl acetate-stained gap junctions by cross-correlating with a reference consisting of a regular six-around-one connexon array (Figs. 3–5). The use of a regular lattice array as reference naturally biases the correlation average toward the most regularly packed portions of the gap junction. Nevertheless, the seven connexon reference can be used to distinguish localized differences in orientation and staining.

Skewing of the six-lobed connexon pairs in the gap junction lattice has been accounted for by interlocking of the lobes in the hexagonal arrays (Baker et al., 1983; Makowski et al., 1984). Thus, regularly packed hexagonal domains were expected to consist of connexons all skewed with the same hand, with the hexamer lobes oriented either to the right or left of the lattice vectors by 8–9°. The Fourier averages appeared to confirm this expectation, but the correlation averages with right- and left-skewed seven connexon references (Fig. 3) showed that lattice domains often contain a subpopulation of connexons skewed opposite to the majority. Because the skewing is attributed to interlocking, it is appropriate to use a small interlocked array as reference for the cross-correlation identification. It is not surprising that there are some overlaps in the cross-correlation maps for the left- and right-skewed references (Fig. 5 F), corresponding to regions where the arrangement of the connexons closely fits that of the average of the two references. The occurrence of regions with opposite skew to the majority may be accounted for by lattice defects, such as those revealed by mapping positions with a single connexon reference (Fig. 7), which could correspond to regions where regular interlocking is not maintained. Using similar cross-correlation methods to analyze the orientation of the triangular porin images in lattice arrays, Dorset et al. (1989) distinguished trigonal and orthorhombic domains bounded by less-ordered regions.

Visual examination of high-contrast micrographs of negatively stained gap junctions (Baker et al., 1985) indicated that there may be large, uncorrelated variations

in the axial stain accumulation among connexons in well-ordered arrays. With the uranyl-stained specimens, differences in axial staining could be distinguished by correlating with seven connexon references (Fig. 4), although it was not possible to use a single connexon reference. The use of the seven connexon references with dark and light centers selects for regions where there is some local correlation in stain accumulation or exclusion, or where at least one of the connexons has much more or less axial stain than the average. The fact that dark and light axially stained connexons can be distinguished with relatively little overlap (Fig. 5 *C*) demonstrates that there are substantial variations in the axial accumulation of uranyl stains. Single particle averaging of connexon images from a methylamine tungstate-stained specimen in which there was, on the average, little axial staining (in contrast to most uranyl-stained specimens), also showed considerable variation in the axial stain accumulation (Fig. 6). These observations suggest that connexon gates may generally be closed in these specimens, and that the opening or collapse of the gates may be more probable in the presence of uranyl than with the tungstate stains, but there are large local variations in the axial accumulation with both types of stain.

Disorder in connexon packing

The reliability of the position determination of the connexon units using the single-particle reference (Fig. 7) was demonstrated by the self consistency of the shape and orientation of the connexon image obtained with different starting references (Fig. 6), which select units at different positions in the lattice. If the positions measured were not reliable, the average images for the different sets would not be so strongly correlated. The displacement errors in the location of the connexon centers due to the noise in the CC peak values thus appear to be small compared to the actual disordered displacements from regular hexagonal packing. Along the horizontal lattice direction in Fig. 8 *B* (vertical in Fig. 7), the connexon centers lie on jaggedly continuous rows, but, in the directions inclined at ±60°, several dislocations are evident that disrupt the hexagonal lattice continuity.

The rms variation in the nearest neighbor pair separation, as measured both from the circularly averaged Fourier transform (Fig. 8 *D*) and the autocorrelation function along the horizontal direction (Fig. 8, *E* and *F*), was ~11% of the mean lattice constant. Furthermore, the rms variation in the *n*th neighbor pair separation increases linearly with distance, unlike an ideal crystal, but the hexagonal lattice orientation is maintained over large distances. This type of two-dimensional packing, intermediate between a liquid and a crystal, that conserves long-range hexagonal orientational order without long-

range translational order has been called "hexatic" (Nelson and Halperin, 1979). Such hexatic ordering is characteristic of moderately close-packed colloidal systems of identical particles, interacting with only repulsive forces, such as polystyrene latex spheres (Murray and Van Winkle, 1987). Very tight packing of the colloidal particles leads to long-range crystalline hexagonal order, and a looser packing results in two-dimensional liquidlike order. The physical parameter that defines the state of such systems is the ratio of effective area (or diameter) of the structural unit to the average area occupied (or mean particle separation).

Under physiological conditions, the mean distance between connexons in junction plaques is >100 Å (Hirokawa and Heuser, 1982), and the connexon arrangement is liquidlike. Analysis of the pair correlation function from freeze-fracture images of such liquidlike arrays showed that the interconnexon interaction is repulsive (Abney et al., 1987); and the concentration of the connexons in the junction plaques has been explained as due to a balance of the interconnexon repulsion and an overall repulsion between the coupled cells that tends to minimize the junctional contact area (Braun et al., 1984).

Isolation of the junction plaques involves removal of some of the membrane lipid, which drives the connexons closer together into hexagonally ordered arrays (Caspar et al., 1977). Mean lattice constants for isolated gap junction lattices prepared under different conditions range from 75–90 Å (Makowski et al., 1984; Caspar et al., 1988). The tightness of the packing in these specimens appears to be due to a balance of the short-range interconnexon repulsion and the forces leading to extrusion of lipid from the membrane plaques. In some close-packed specimens with reduced lipid content, long-range crystalline ordering of the connexons has been observed, but the irregular hexagonal packing illustrated in Figs. 7 and 8 is more typical of isolated junction plaques. The short-range repulsion, impeding close packing of the connexons, may be attributed to boundary lipid, analogous to bound water in hydrated molecules that prevents close contact (Israelachvili, 1985). Although there is considerable disorder in the junction lattice (Figs. 7 and 8), the packing may be tight enough to account for the regular skewed orientation of the connexons (Fig. 6) as a result of interlocking of the hexagonal lobes.

REFERENCES

Abney, J. R., J. Braun, and J. C. Owicki. 1987. Lateral interactions among membrane proteins. Implications for the organization of gap junctions. *Biophys. J.* 52:441–454.

Baker, T. S. 1981. Image processing of biological specimens: a bibliography. *In* Electron Microscopy in Biology. J. D. Griffith, editor. John Wiley and Sons Inc., New York. 189–290.

Baker, T. S., D. L. D. Caspar, C. J. Hollingshead, and D. A. Goodenough. 1983. Gap junction structures. IV. Asymmetric features revealed by low irradiation microscopy. *J. Cell Biol.* 96:204–216.

Baker, T. S., G. E. Sosinsky, D. L. D. Caspar, C. Gall, and D. A. Goodenough. 1985. Gap junction structures. VII. Analysis of connexon images obtained with cationic and anionic negative stains. *J. Mol. Biol.* 184:81–98.

Bennett, M. V. L., and D. A. Goodenough. 1978. Gap junctions, electronic coupling, and intercellular communications. *Neurosci. Res. Program Bull.* 16:375–486.

Braun, J., J. R. Abney, and J. C. Owicki. 1984. How a gap junction maintains its structure. *Nature (Lond.).* 210:316–318.

Caspar, D. L. D., D. A. Goodenough, L. Makowski, and W. C. Phillips. 1977. Gap junction structures. I. Correlated electron microscopy and x-ray diffraction. *J. Cell Biol.* 74:605–628.

Caspar, D. L. D., G. E. Sosinsky, T. T. Tibbitts, W. C. Phillips, and D. A. Goodenough. 1988. Gap junction structure. *In* Gap Junctions. E. Hertzberg and R. Johnson, editors. Alan R. Liss Inc., New York. 117–133.

Crepeau, R. H., and E. K. Fram. 1981. Reconstruction of imperfectly ordered zinc-induced tubulin sheets using cross-correlation and real space averaging. *Ultramicroscopy.* 6:7–18.

Dorset, D., A. K. Massalski, and J. P. Rosenbusch. 1989. In-plane phase transition of an integral membrane protein: nucleation of the OmpF matrix porin rectangular polymorph. *Proc. Natl. Acad. Sci. USA.* 86:6143–6147.

Frank, J. 1982. New methods for averaging non-periodic objects and distorted crystals in biological electron microscopy. *Optik.* 63:67–89.

Frank, J., W. Chiu, and L. Degn. 1988. The characterization of structural variations within a crystal field. *Ultramicroscopy.* 26:345–360.

Henderson, R. H., J. M. Baldwin, K. H. Downing, J. Lepault, and F. Zemlin. 1986. Structure of purple membrane from *Halobacterium halobium:* recording, measurement and evaluation of micrographs at 3.5 Å resolution. *Ultramicroscopy.* 19:147–178.

Hirokawa, N., and J. Heuser. 1982. The inside and outside of gap-junction membranes visualized by deep etching. *Cell.* 30:395–406.

Israelachvili, J. N. 1985. Intermolecular and Surface Forces with Applications to Colloidal and Biological Systems. Academic Press Limited (AP), London. 1–296.

Makowski, L., D. L. D. Caspar, W. C. Phillips, T. S. Baker, and D. A. Goodenough. 1984. Gap junction structures. VI. Variation and conservation in connexon conformation and packing. *Biophys. J.* 45:208–218.

Manella, C. A., and J. Frank. 1984. Negative staining characteristics of arrays of mitochondrial pore protein: use of correspondence analysis to classify different staining patterns. *Ultramicroscopy.* 13:93–102.

Manella, C. A., A. Ribeiro, and J. Frank. 1986. Structure of the channels in the outer mitochondrial membrane: electron microscopic studies of the periodic arrays induced by phospholipase A_2 treatment of the Neurospora membrane. *Biophys. J.* 49:307–318.

Murray, C. A., and D. H. Van Winkle. 1987. Experimental observation of two-stage melting in a classical two-dimensional screened coulomb system. *Phys. Rev. Lett.* 58:1200–1203.

Nelson, D. R., and B. I. Halperin. 1979. Dislocation-mediated melting in two dimensions. *Phys. Rev. B.* 19:2457–2484.

Saxton, W. O., and W. Baumeister. 1982. The correlation averaging of a regularly arranged bacterial cell envelope protein. *J. Microsc. (Oxf.).* 127:127–138.

Sosinsky, G. E., J. C. Jesior, D. L. D. Caspar, and D. A. Goodenough. 1988. Gap junction structures. VIII. Membrane cross-sections. *Biophys. J.* 53:709–722.